Received: 14 March 2019 | Revised: 19 August 2019 | Accepted: 16 September 2019

DOI: 10.1002/jbm.b.34495

Society For Biomaterials WILEY

ORIGINAL RESEARCH REPORT

Size matters: Effect of granule size of the bone graft substitute (Herafill®) on bone healing using Masquelet's induced membrane in a critical size defect model in the rat's femur

Maximilian Leiblein[1] | Elias Koch[1] | Andreas Winkenbach[1] | Alexander Schaible[1] | Christoph Nau[1] | Hubert Büchner[2] | Katrin Schröder[3] | Ingo Marzi[1] | Dirk Henrich[1]

[1]Klinik für Unfall-, Hand- und Wiederherstellungschirurgie, Klinikum der Johann Wolfgang Goethe-Universität, Frankfurt am Main, Germany

[2]Heraeus Medical GmbH, Wehrheim, Germany

[3]Vascular Research Center, University of Frankfurt, Frankfurt am Main, Germany

Correspondence
Maximilian Leiblein, Department of Trauma Surgery, Johann-Wolfgang-Goethe University Hospital, Theodor-Stern-Kai 7, 60590 Frankfurt, Germany.
Email: maximilian.leiblein@kgu.de

Funding information
Heraeus Medical GmbH, Wehrheim, Germany

Abstract

The Masquelet technique for the treatment of large bone defects is a two-stage procedure based on an induced membrane. The size of a scaffold is reported to be a critical factor for bone healing response. We therefore aimed to investigate the influence of the granule size of a bone graft substitute on bone marrow derived mononuclear cells (BMC) supported bone healing in combination with the induced membrane. We compared three different sizes of Herafill® granules (Heraeus Medical GmbH, Wehrheim) with or without BMC in vivo in a rat femoral critical size defect. A 10 mm defect was made in 126 rats and a membrane induced by a PMMA-spacer. After 3 weeks, the spacer was taken out and membrane filled with different granule sizes. After 8 weeks femurs were taken for radiological, biomechanical, histological, and immunohistochemical analysis. Further, whole blood of the rat was incubated with granules and expression of 29 peptide mediators was assessed. Smallest granules showed significantly improved bone healing compared to larger granules, which however did not lead to an increased biomechanical stability in the defect zone. Small granules lead to an increased accumulation of macrophages in situ which could be assigned to the inflammatory subtype M1 by majority. Increased release of chemotactic respectively proangiogenic active factors in vitro compared to syngenic bone and beta-TCP was observed. Granule size of the bone graft substitute Herafill® has significant impact on bone healing of a critical size defect in combination with Masquelet's technique in terms of bone formation and inflammatory potential.

KEYWORDS

bone marrow derived mononuclear cells, critical size defect, induced membrane, Masquelet technique, scaffold size

1 | INTRODUCTION

The treatment of critical size bone defects resulting from tumor resections, osteomyelitis, or trauma poses a huge challenge for surgeons and patients (Wiese & Pape, 2010). Those defects are defined as bone loss greater than 50% of the circumference of the particular bone. Alternatively, they are described as an "intraosseous wound in a particular bone and species of animal that will not heal during the lifetime of the animal or a defect that shows less than 10% regeneration during the animal's lifetime" (Schemitsch, 2017).

Different surgical options are available, such as autologous bone grafting, bone transport (distraction osteogenesis) or vascularized free

bone transfer (Giannoudis, Faour, Goff, Kanakaris, & Dimitriou, 2011). All of those techniques contain limitations, such as restricted bone volume at the donor site and donor site morbidity such as long lasting pain (Nau et al., 2016; Seebach et al., 2015).

As an alternative Masquelet et al. described a two-stage procedure for the treatment of large bone defects based on an induced membrane (Masquelet, Fitoussi, Begue, & Muller, 2000).

In the first step, a fibrous membrane is induced around the defect by implanting a PMMA spacer into the defect. After 6–8 weeks, a second operative step follows, the induced membrane is opened and the spacer taken out. The thus originated cavity is filled with either spongious bone or a scaffold.

Masquelet et al. found the main mechanism of action of the induced membrane in the prevention of resorption of the graft and secretion of growth-factors. The membrane serves as a "bioreactor," building a barrier against the surrounding soft tissue (Masquelet & Begue, 2010).

However, in previous work our group demonstrated that multiple factors influence the development and quality of the induced membrane. We were able to show, that different sorts of cement and additive antibiotics have a significant influence on the development of the membrane (Nau et al., 2016).

Furthermore, we demonstrated that the cellular composition and growth factor content of the induced membrane is highly dependent on its age and subsides after 6 weeks (Henrich et al., 2016).

It has been shown by multiple groups, that autologous cancelleous bone graft can be replaced by synthetic scaffolds such as tricalcium phosphate, hydroxyapatite or demineralized bone matrix to fill the defect if combined with an osteoinductive agent such as bone marrow-derived mononuclear cells (BMC) (Bosemark, Perdikouri, Pelkonen, Isaksson, & Tägil, 2015; Donegan, Scolaro, Matuszewski, & Mehta, 2011; Gupta et al., 2016; Moghaddam, Zietzschmann, Bruckner, & Schmidmaier, 2015; Seebach, Schultheiss, Wilhelm, Frank, & Henrich, 2010).

Evidence is reported, that the size of a scaffold granule is a critical factor for bone healing response (Coathup, Cai, Campion, Buckland, & Blunn, 2013; Ghanaati et al., 2010; Jensen et al., 2015; Klüppel et al., 2013; Kon, Shiota, Ozeki, & Kasugai, 2014; Malinin, Carpenter, & Temple, 2007; Maté Sánchez de Val et al., 2016; Shapoff, Bowers, Levy, Mellonig, & Yukna, 1980; Sun et al., 1999). The reason for this is expected in a different surface-to-volume ratio. Size and packing density between the granules play an important role for bone formation by influencing the three-dimensional structure of the scaffold. Depending on the packing density nutrients, cells and blood vessels are able to immigrate into the defect (Coathup et al., 2013). On the other hand, higher mechanical stability can be achieved with tighter packing (Putzer, Coraça-Huber, Wurm, Schmoelz, & Nogler, 2014). Furthermore, the granule size has important impact on material dissolution and resorption characteristics (Klüppel et al., 2013).

Herafill® (Heraeus Medical GmbH, Werheim) is a bioresorbable bone void filling material. The primary component of Herafill® is calcium sulfate, combined with calcium carbonate, triglyceride, and gentamicin (Heraeus Medical GmbH, 2017).

Currently Herafill® is mainly used as a carrier for antibiotics (Coraça-Huber et al., 2015). Possible indications contain the treatment of osteomyelitis (Franceschini, Di Matteo, Bösebeck, Büchner, & Vogt, 2012; Gramlich, Walter, Gils, & Hoffmann, 2017), perioperative infections (Pförringer et al., 2016) as well as periprosthetic joint infections (Marczak, Synder, Sibiński, Okoń, & Kowalczewski, 2016). In a clinical trial using Herafill® as biomaterial for the treatment of osteomyelitis, it showed excellent properties as a carrier for antibiotics in the context of septic indications, but also inducing new bone formation (Seyler et al., 2010).

To the best of our knowledge, there are no data published concerning the influence of the granule size on bone healing in concert with Masquelet's induced membrane technique. In the present study, we therefore analyzed the influence of the granule size of Herafill® on BMC supported bone healing in combination with the induced membrane technique in a rat critical size defect model.

We hypothesized that a range of granule sizes exists which supports bone healing to a special degree and that addition of BMC leads to further improvement of defect healing.

2 | MATERIALS AND METHODS

2.1 | Ethics and animal care

All animal experiments were performed in accordance with regulations set forth by our institution's animal care and oversight committee (Project No. FK/K1053 Regierungspräsidium, Darmstadt, Germany) in accordance to German law. One-hundred and twenty-six 12-week old male Sprague–Dawley rats (Janvier, Le Genest-Saint-Isle, France), weighing approximately 350–400 g were housed in individual cages, in temperature 21.8°C), air flow and light-controlled (12 hr day and 12 hr night) rooms and received rat food and water ad libitum. Animals were monitored daily in the postoperative period (5 days) for signs of pain, discomfort, and complications.

2.2 | Biomaterial characterization (Herafill®)

Herafill® (Heraeus Medical GmbH, Wehrheim) is a bioresorbable bone void filling material. The primary component of Herafill® is calcium sulfate, combined with calcium carbonate, triglyceride, and gentamicin (Heraeus Medical GmbH, 2017). Three different ranges of granule sizes of Herafill® were used as scaffold (0.5–1 mm, 1–3 mm, 3–5 mm). The material was kindly provided by Heraeus Medical (Wehrheim, Germany). To analyze the surface characteristics, untreated granules of each size were assessed by using a scanning electron microscope. The samples were sputtered with gold (3 × 60 s, Agar Sputter Coater, Agar Scientific, Ltd., UK) and analyzed using a Hitachi FE-SEM S4500 (Hitachi, Dusseldorf, Germany) with a voltage of 5 kV. The images were digitally recorded using the Digital Image Processing System 2.6 (Point Electronic, Halle, Germany).

2.3 | Bone marrow-derived mononuclear cells (BMC)

Femurs were surgically taken from donor rats, bone marrow was flushed from the medullary cavity and diluted with phosphate-buffered

saline (PBS 1:3). Mononuclear cells were isolated by density gradient with *Ficoll* at 800 g for 20 min without brake at room temperature. Afterwards, mononuclear cells were washed twice with PBS and counted.

In order to seed BMC onto Herafill®, scaffolds were placed in a monolayer in individual wells (area = 2 cm^2) and syngenic BMC in a volume of 350 µL PBS were dripped onto the scaffolds (concentration: $1.33 \times 10^6/cm^3$ biomaterial) (Seebach et al., 2015; Seebach et al., 2016; Verboket et al., 2018). Afterwards an incubation at 37°C followed for 10 min. The medium containing nonadherent cells was subsequently removed and dripped again onto the scaffolds and incubated as before. This procedure was repeated once more.

To ensure a sufficient concentration of BMC at the defect site, the suspension with nonadherent BMC was concentrated to a volume of 50 µL and carefully dripped onto the implanted scaffolds. Due to the membrane, the nonadherent cells stayed at the defect site.

In order to measure the BMC-adherence to the Herafill®-scaffold some of the granules (small size, 0.5–1 mm) seeded with BMC were fixed in formaldehyde solution (0.5%, 10 min, room temperature). After removing the formaldehyde solution, samples were washed three times with PBS and DAPI (4′,6-diamidino-2-phenylindole) was added (1 µg/ml in PBS) (Life Technologies, Darmstadt, Germany). After 5 min, the DAPI solution was removed and samples were washed three times with 1 ml PBS each time. Adherence was then assessed by directly viewing the samples with fluorescence microscopy using a Zeiss *Axioobserver Z1* (Zeiss, Göttingen, Germany) (Figure 1d).

2.4 | Surgical procedure

Surgical procedure was performed as described in earlier work of our group (Henrich et al., 2009; Nau, Seebach, et al., 2016; Nau et al., 2018; Seebach, Henrich, Wilhelm, Barker, & Marzi, 2012; Seebach et al., 2010; Seebach et al., 2015). Under general intraperitoneal anesthesia (Ketavet 70 mg/kg and Rompun 10 mg/kg) the right leg was shaved, cleaned, and disinfected and animals were placed in a lateral position. A longitudinal incision was made in the skin and the fascia over the right femur. The biceps femoris and vastus lateralis muscles were separated bluntly exposing the anterolateral aspect of the femoral bone. A 6-hole, 1.5 mm stainless-steel mini-plate (LCP compact hand 1.5 straight, Depuy-Synthes, Dubendorf, Switzerland, catalog number 036.000.038) was applied to the anterior aspect of the femur shaft and secured in place with two proximal and two distal 1.5 mm cortical screws (Synthes, CompactHand). After stabilization, a critical size defect (CSD), measuring 10 mm, was created in the femur bone shaft, underneath the plate using a Gigli saw (RI-Systems, Davos, Switzerland). The cement was hand mixed according to the manufacturer's protocol. The bone defect was then filled with the respective PMMA (Palacos R + G) cement and molded into a cylindrical shape. The wound was irrigated

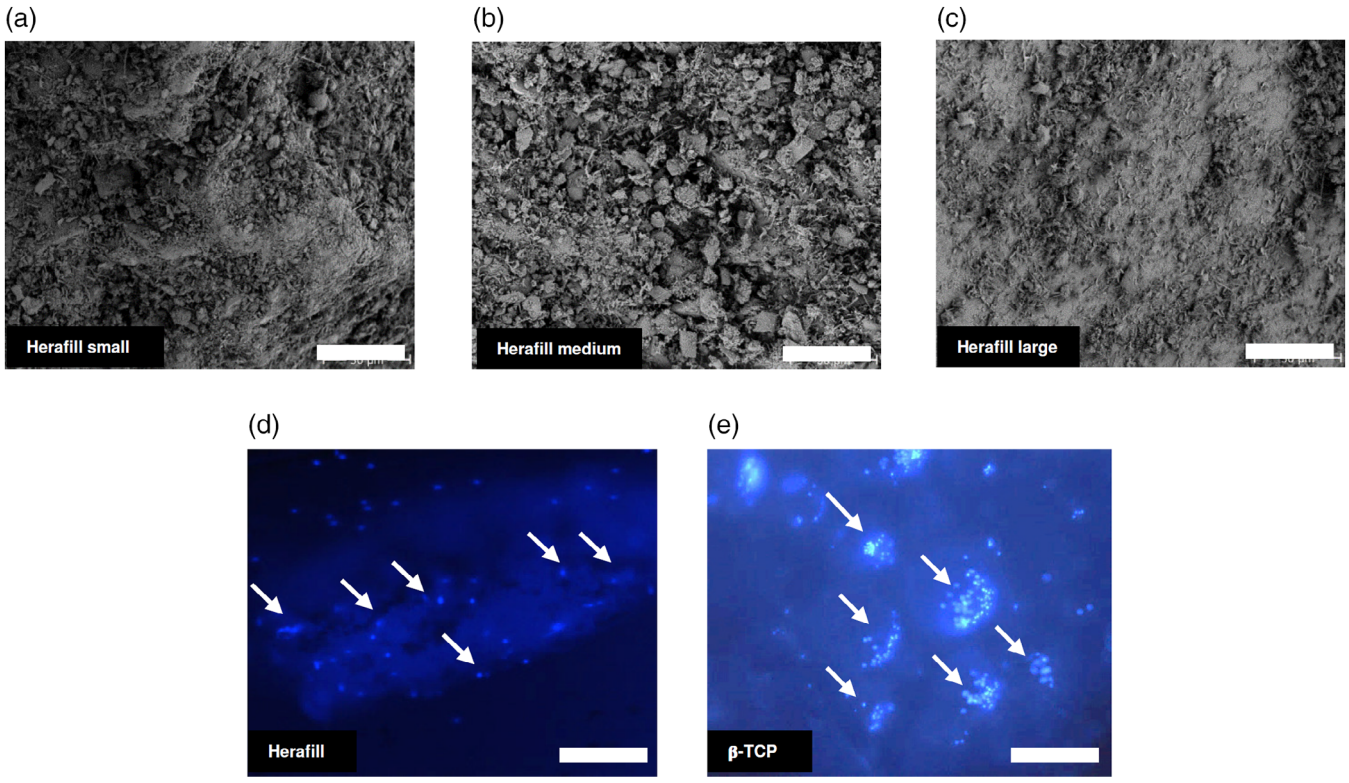

FIGURE 1 Surface structure of Herafill® granulates determined by SEM. Herafill® demonstrates a ruffled surface with irregular structures in the µm-range (a–c). Attachment of BMC to Herafill® granulate (d) and beta-TCP (e) (historic control) as revealed by DAPI-staining and fluorescence microscopy. Cells show a distinct better adherence when seeded on beta-TCP (e) compared to Herafil® (d). Arrows mark attached BMC. White bar represents 50 µm (a, b, c) and 100 µm (d, e)

with sterile saline, the fascia was reapproximated with interrupted 5–0 Vicryl sutures, and the superficial fascia and skin closed with Prolene 5-0 suture (Ethicon, Germany). Animals were returned to their cages, monitored daily for the occurrence of abnormal behavior or complications and analgesia was given for 7 days postoperatively.

Three weeks after the initial operation the induced membrane surrounding the defect/PMMA (Palacos R + G) cement spacer was opened and the spacer was taken out and weighed. The membrane was filled with Herafill®-granules (small 0.5–1.0 mm/medium 1.0–3.0 mm/large 3.0–5.0 mm) or autologous cancellous bone with or without BMC. The weight of the implanted scaffold was measured by difference of in- and out-load of the previously weighed unit. Afterwards the membrane was closed with interrupted 5-0 Vicryl sutures and the wound was closed as previously described. The operative approach and the postoperative aftercare were performed as in the initial operation.

Eight weeks after the second operation animals were sacrificed with an overdose (500 mg/kg) of pentobarbital intraperitoneally administered. The femora were removed carefully from both sides, wrapped into wet gaze, and stored at −80°C until further processing.

For μCT-analysis, femurs were defrosted and stored in 70% alcohol. Subsequently those bones were used for biomechanical testing. Contralateral bones were treated equivalently and served as reference for biomechanical evaluation.

For histological analysis, femurs were decalcified and fixed in 10% formalin solution for later paraffin embedding.

2.5 | Treatment groups

One hundred and twenty-six animals were operated and allocated into seven groups (n = 18 animals/group) depending on defect filling; 24 additional animals were sacrificed to serve as donors for syngenic bone and BMC.

2.6 | Evaluation

2.6.1 | μCT analysis

To assess bone mineral density and callus volume μCT analysis was performed with a high-resolution in-vivo-micro-CT Skyscan 1176 (Bruker AXS, Karlsruhe, Germany). The long axis of the femur was lined up orthogonally to the axis of the X-ray beam (Al 0.5 mm; voltage: 50 kV; current: 500 μA; frame average: 7; rotation ra.: 180; rotation st.: 0.5) and the region of interest was placed on the defect. Isotropic voxel size was 18 μm^3. Two-dimensional CT-images were scanned, reconstructed using a standard back convolution procedure, and saved in 3D arrays.

2.6.2 | Biomechanical testing

Bones that had already been used for evaluation in μCT were analyzed biomechanically in a destructive three-point bending procedure using material testing machine (Zwickiline Z5.0, Zwick-Roell, Ulm, Germany). Between both procedures, bones were stored in 70% ethanol. The "bending until failure" was performed by lowering a bar onto the bone. Distance between the settings was 20 mm, speed of deflection was 0.1 mm/s and load and deflection were recorded constantly. Point of failure was defined as maximum load followed by quick load reduction of 50%. Ultimate load and stiffness (slope of the elastic deformation part of the load/deformation curve) were calculated using the Testexpert-II software (Zwick-Roell). Contralateral femora were used as control and data were presented as percentage of ultimate load of the corresponding contralateral femur (Seebach, Henrich, et al., 2010).

2.6.3 | Histological analysis

For histological analysis, 6–8 femurs per group were defrosted and fixed in 10% Zinc-Formal-Fixx (Thermo Electron, Pittsburgh) for 20 hr. Subsequently decalcification in 0.25 M Trizma base (Sigma–Aldrich) and 10% EDTA, pH 7.4, followed. Decalcified femurs were paraffin-embedded and cut in sections (3 μm) parallel to their long axis.

Movat's pentachrome staining was performed as described by Garvey et al. using a staining kit (Morphisto, Frankfurt, Germany) (Garvey, Fathi, Bigelow, Carpenter, & Jimenez, 1986).

Vascularization was measured using α-SMA-staining. Sections were incubated with mouse anti-rat α-SMA (antibody-ID: AB_262054, clone 1A4, final concentration 2 μG/ml, 1 hr at room temperature, Abcam, Cambridge, UK).

Macrophages were measured using mouse anti-rat antibodies against CD68+ cells (antibody ID: AB_307338, clone KP1, final concentration 2 μG/ml, 1 hr at room temperature, Abcam). For detection of M1 macrophages, slides were incubated 1 hr with monoclonal mouse anti-rat 163 (antibody ID: AB_1287939, clone ED2, 0.5 mG/ml, dilution 1:75, 1 hr at room temperature, Bio-Techne, Wiesbaden, Germany). A polyclonal rabbit anti rat CD80 antibody was uses to stain M2 macrophages (antibody ID: AB_10859698, 1 mG/ml, dilution 1:250, 1 hr at room temperature, Bioss Antibodies, Biozol, Eching, Germany).

In all stainings as secondary antibody a polyclonal HRP conjugated anti-mouse or anti rabbit IgG (Simple Stain Rat MAX PO, Nichirei, Tokyo, Japan) was applied for 30 min followed by incubation with 3-amino-9-ethylcarbazole (AEC, Sigma). Finally, a counterstain with hematoxylin was performed.

Furthermore, a qualitative analysis of the bone healing result based on the Movat's pentachrome stained slides was performed. For this analysis, the numbers of totally bridged (both corticalis were spanning the defect), partially bridged (corticalis on one side was spanning the defect), and marginally bridged defects (poor new bone formation in the cortical area and inner defect area) were evaluated.

High-resolution pictures of the complete defect were created by automatized linking of singular pictures using the microscope *Biorevo BZ-9000* (Keyence, Neu-Isenburg, Germany) and the software BZII Analyzer (Keyence, Neu-Isenburg, Germany). For further details the microscope *Axioobserver Z1* (Zeiss, Göttingen, Germany) was used.

New bone formation, respectively α-SMA-positive areas, was assessed using the software *ImageJ* (Rasband, W.S., ImageJ, U.S. National Institutes of Health, Bethesda, MD, https://imagej.nih.gov/ij/, 1997–2018) as described previously (Henrich et al., 2018; Janko et al., 2019), and the percentage of α-SMA-positive area of the defect zone was calculated.

The relative frequency of CD68+ macrophages was assessed using a relative scale from 0 (none) to 3 (frequently) in five areas per defect at 400-fold magnification.

2.6.4 | Analysis of inflammatory potential

For this experiment 0.5 ml heparinized whole blood of the rat, diluted with serum-free medium in a ratio of 1:1 was mixed with either 100 µL Herafill® small (0.5–1.0 mm), beta-TCP (Chronos®, size 0.7–1.4 mm, DePuy Synthes, Umkirch, Germany) or syngenic bone (freshly harvested and minced to small pieces of approximately 1 mm) and incubated for 24 hr at 37°C.

Supernatent was harvested by centrifugation (15 min, 2,000 g) and the expression of 29 different peptide mediators was assessed using a proteome-profiler system (Proteom Profiler Rat Cytokine Array Kit, Panel A, RnD-Systems, Wiesbaden, Germany) following the instructions of the manufacturer. Density of spots in relation to control spots with known protein concentration was evaluated using *ImageJ*. This experiment was performed twice. Multiple publications are available using the kit successfully for the analysis of rat cytokines (Afroz et al., 2019; Cizkova et al., 2018; Elgström, Ohlsson, & Eriksson, 2017).

2.7 | Statistics

Results are presented as boxplots of the median, 25% and 75% quartiles, respectively. Whisker indicates minimum and maximum.

Statistical analysis was done with Bias 11.02 (Epsilon-Verlag, Darmstadt, Germany). The power analysis was planned to detect differences in histological evaluation of bone mass increase (based on Movat's pentachrome staining) between four experimental groups (syngenic bone, small, medium, large granules). Based on previous comparable studies (Janko et al., 2017; Nau et al., 2018; Seebach et al., 2015), a pooled standard deviation of 25% and a power of 80% were considered to detect true differences in means of 45% between the treatment groups at a level of two-sided significance of 5%. These considerations resulted in a group size of $n = 8$ for histology groups.

Nonparametric Kruskal–Willis test with Bonferroni-Holm corrected post hoc analysis was used to compare differences between the groups. The categorial data was statistically analyzed using Fisher's exact test.

p-values below .05 were considered statistically significant, *p*-values between .05 and .1 were valued as a statistical trend.

3 | RESULTS

3.1 | Surface characterization of the scaffold and cell adhesion

The SEM analysis of the surface revealed both plain and rough areas. While small (0.5–1 mm) and especially medium (1–3 mm) granules showed a clefty surface with partially columnar shaped structures, large granules (3–5 mm) had bigger areas with plain surface. Irregular structures were predominant in all granule sizes (Figure 1a–c).

DAPI staining showed adherence of BMC to granules. Degree of adherence was low in relation to BMC seeded on beta-TCP under the same conditions (concentration and seeding procedure) (Figure 1d,e). A historic group served as control, direct comparison was not carried out.

3.2 | Complications

Of the 126 animals that underwent surgery, 21 had to be excluded. During surgery 13 animals died due to breathing arrest, one animal suffered femur fracture during implantation of the plate, one femur fractured during explantation. In the postoperative course, six animals showed an infection. The number of complications is comparable with those of earlier studies (Warzecha et al., 2013).

Analyzing the bodyweight, all animals in all groups showed physiologically weight gain.

3.3 | Low biomechanical properties in all groups

Biomechanical testing showed significantly lower bending stiffness in all treatment groups compared to control (Figure 2). Addition of BMC did not lead to an increased bending stiffness.

Analyzing the ultimate load with a destructive three-point bending procedure, treated femora showed low biomechanical stability and were frequently only bent and not fractured. Contralateral, healthy bones fractured and showed the expected results. Therefore, ultimate load results are not shown.

3.4 | Callus formation increased after transplantation of smallest sized biomaterial

Analysis of pentachrome-stained histological slides revealed a distinct callus formation throughout the complete defect area when small

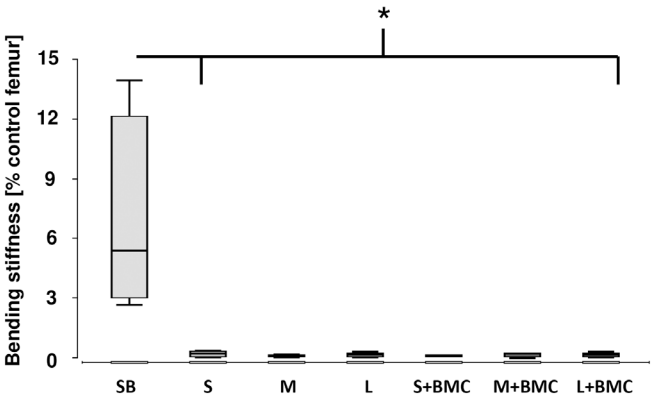

FIGURE 2 Biomechanical strength (bending stiffness) of the defect zones measured by destructive three-point bending test. Values were presented as % of the healthy contralateral femur. Bending stiffness of defects treated with syngenic bone was significantly increased compared to all other groups. *$p < .05$. L, large granules; L + BMC, large granules plus bone marrow derived mononuclear cells; M, medium granules; M + BMC, medium granules plus bone marrow derived mononuclear cells; S, small granules; SB, syngenic bone; S + BMC, small granules plus bone marrow derived mononuclear cells

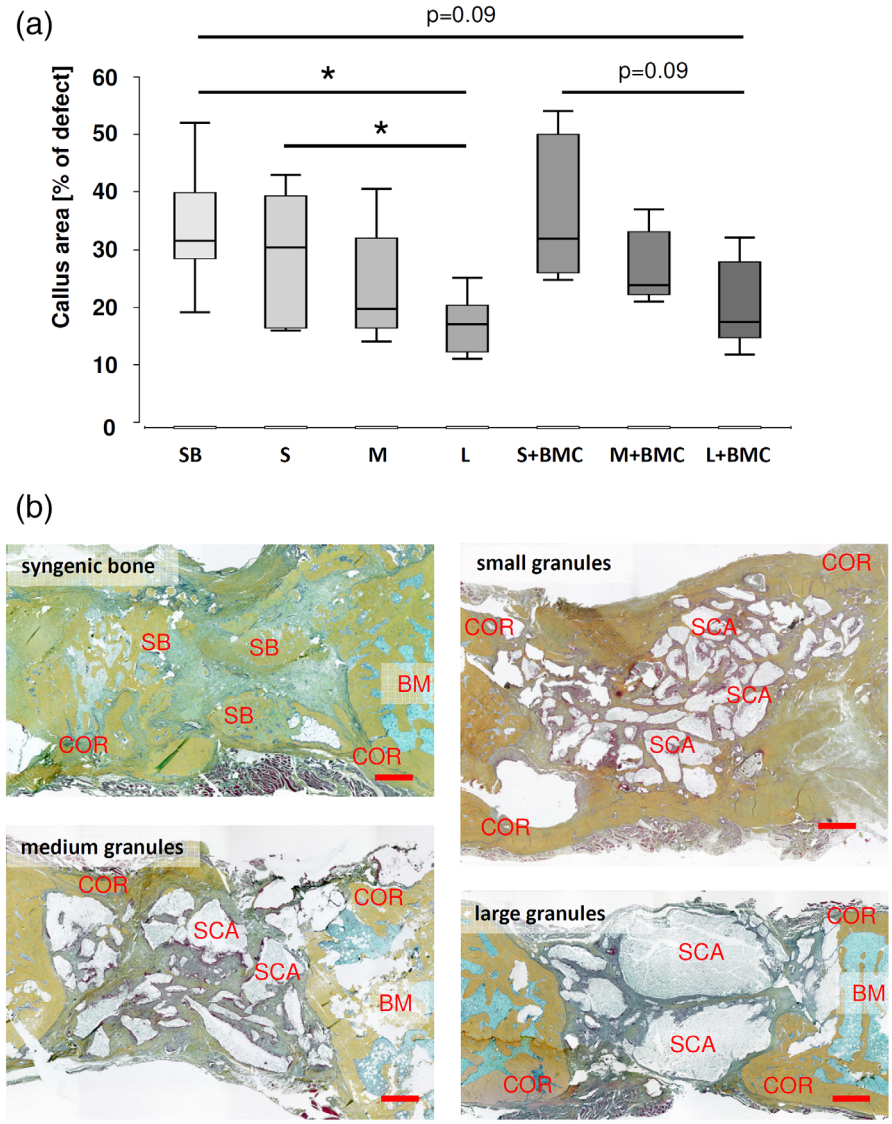

FIGURE 3 Bone tissue in the defect area as assessed by histomorphometric analysis of Movat's pentachrome stained histological slices 8 weeks after surgery (a). Representative images of Movat's pentachrome staining are shown in (b). Bone tissue appears yellow. *$p < .05$. BM, bone marrow; COR, corticalis; SCA, scaffold. Red bar represents a distance of 1 mm. L, large granules; M, medium granules; S, small granules; SB, syngenic bone

Group	No. of animals	Totally bridged[a]	Partially bridged[b]	Marginally bridged[c]
Syn	7	57%	43%	0%
S	6	17%	50%	33%
M	6	0%	83%	17%
L	6	0%	83%	17%
S + BMC	6	33%	50%	17%
M + BMC	7	14%	72%	14%
L + BMC	6	17%	66%	17%

TABLE 1 Percentage of totally bridged, partially bridged, and marginally bridged bone defects in the single treatment groups

Abbreviations: L, large granules; M, medium granules; S, small granules; Syn, syngenic bone.
[a]Cortical bone in histological analysis (2D) spanning the defect on both sides, significant bone formation in the defect.
[b]Cortical bone spanning the defect on one side, bone formation in the defect.
[c]Marginally bone formation at the cortical site and within the defect.

granules were used in the cell free treatment groups. Callus was built in both between the single granules and in the cortical area. With increasing granule size, this effect decreased significantly (Figure 3). A slightly increased, but not significantly higher, callus formation was found when BMC enriched granules were used compared to the cell-free granules. As well as in the cell free groups callus formation was lower when bigger granules were used ($p = .09$) (Figure 3).

The extent of bony bridging in the defect area was analyzed in a qualitative analysis of the slides. Highest rate of completely consolidated defects was found when syngenic bone was used. In groups with BMC

loaded granules a slightly higher rate of completely consolidated defects was found compared to cell free groups (not significant) (Table 1).

Results of the radiological analysis were generally in line with histological findings. Defects filled with syngenic bone demonstrated almost complete consolidation. Defects filled with small granules showed distinct, compartmentalized, partially fused bone formation between granules. Callus formation was also detectable on the surface and between granules when large sized granules were used. For consolidation of the defect, further callus fusion is necessary (Figure 4a). Addition of BMC did not increase callus formation (Figure 4a). Quantitative analysis of μCT-data showed different results. Radiologically quantifiable callus formation was highest in groups with medium-sized granules (data not shown).

The bone mineral density in the defect area was found significantly increased when small granules were used compared to large granules in both with or without BMC ($p < .05$, Figure 4b). Defects

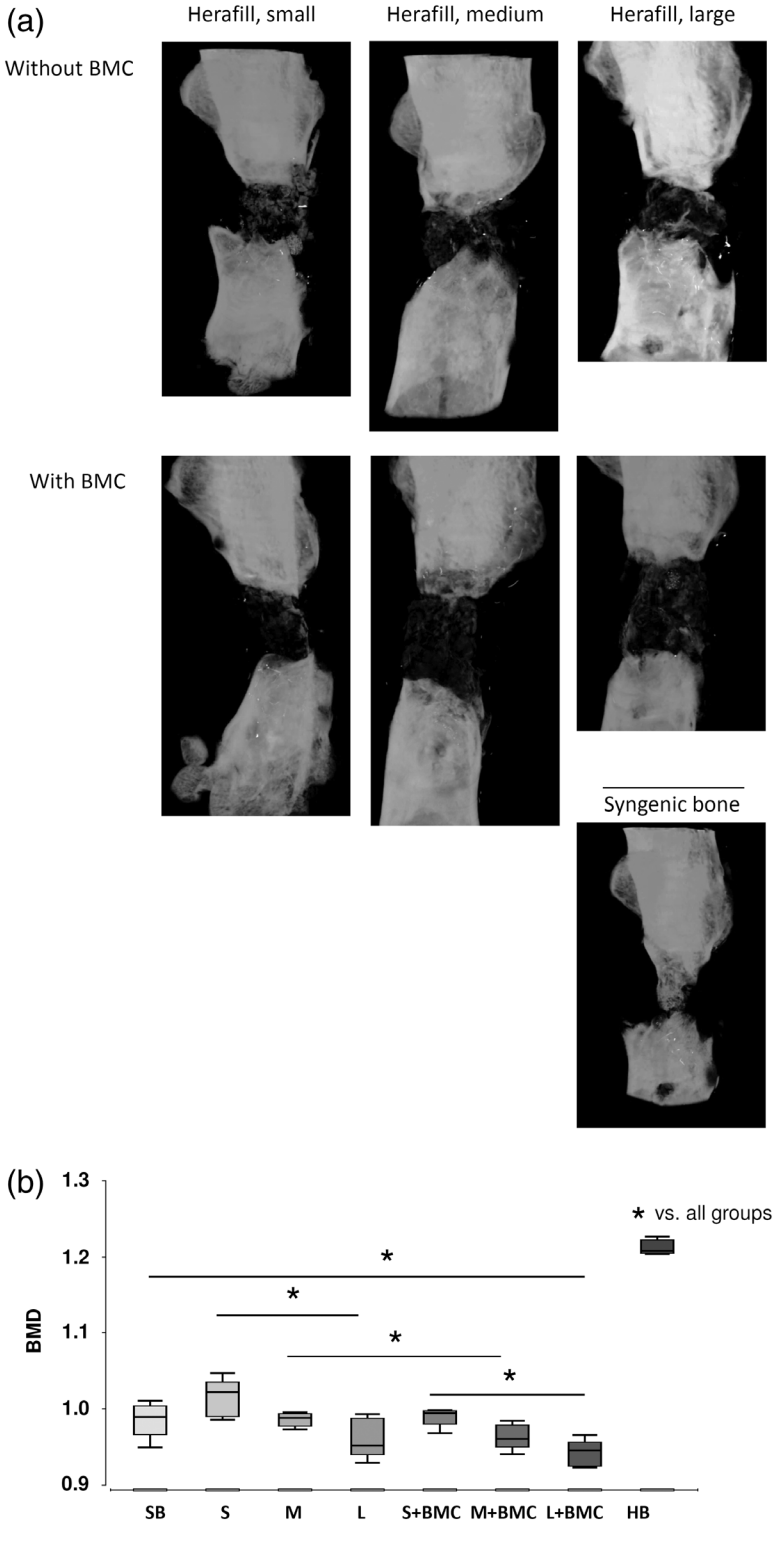

FIGURE 4 Representative micro-CT of defects filled with small, medium and large sized granules ± BMC and of a defect filled with syngenic bone as control 8 weeks after surgery showing bone mineralization and mineralized callus formation in the defect zone (a). Bone mineral density in the defect area in dependency from granule size and addition of BMC (b). HB, healthy bone; L, large granules; M, medium granules; S, small granules; SB, syngenic bone. *$p < .05$

filled with syngenic osseous bone showed a slightly lower median compared to defects filled with small granules.

Compared to healthy bones (contralateral reference bones) bone mineral density was significantly lower in respective defect areas of all treatment groups ($p < .05$, Figure 4b).

Defects filled with BMC loaded granules showed higher BMD when small-sized granules were used compared to medium ($p = .06$) and large-sized ($p < .05$) (Figure 4b).

Comparing defects filled with cell free and BMC loaded granules a significantly decreased BMD was found in BMC groups. Groups with medium-sized granules showed a significant difference ($p < .05$), groups with large granules showed a weak statistical trend ($p = .12$) (Figure 4b).

3.5 | Vascularization

No significant difference of vascularization was found between defects filled with different sized granules (small, medium, large), neither between treatment groups and defects filled with syngenic bone (Figure 5a).

A slightly higher vascularization was found in defects filled with BMC loaded small granules in comparison to cell-free small granules ($p = .09$, Figure 5a).

In general, vessels showed no consistent distribution but were concentrated at the fracture site and in close vicinity to muscle tissue (Figure 5c). Analysis of vessel density per unit area of callus showed significant increase of vessel density in defects filled with large granules

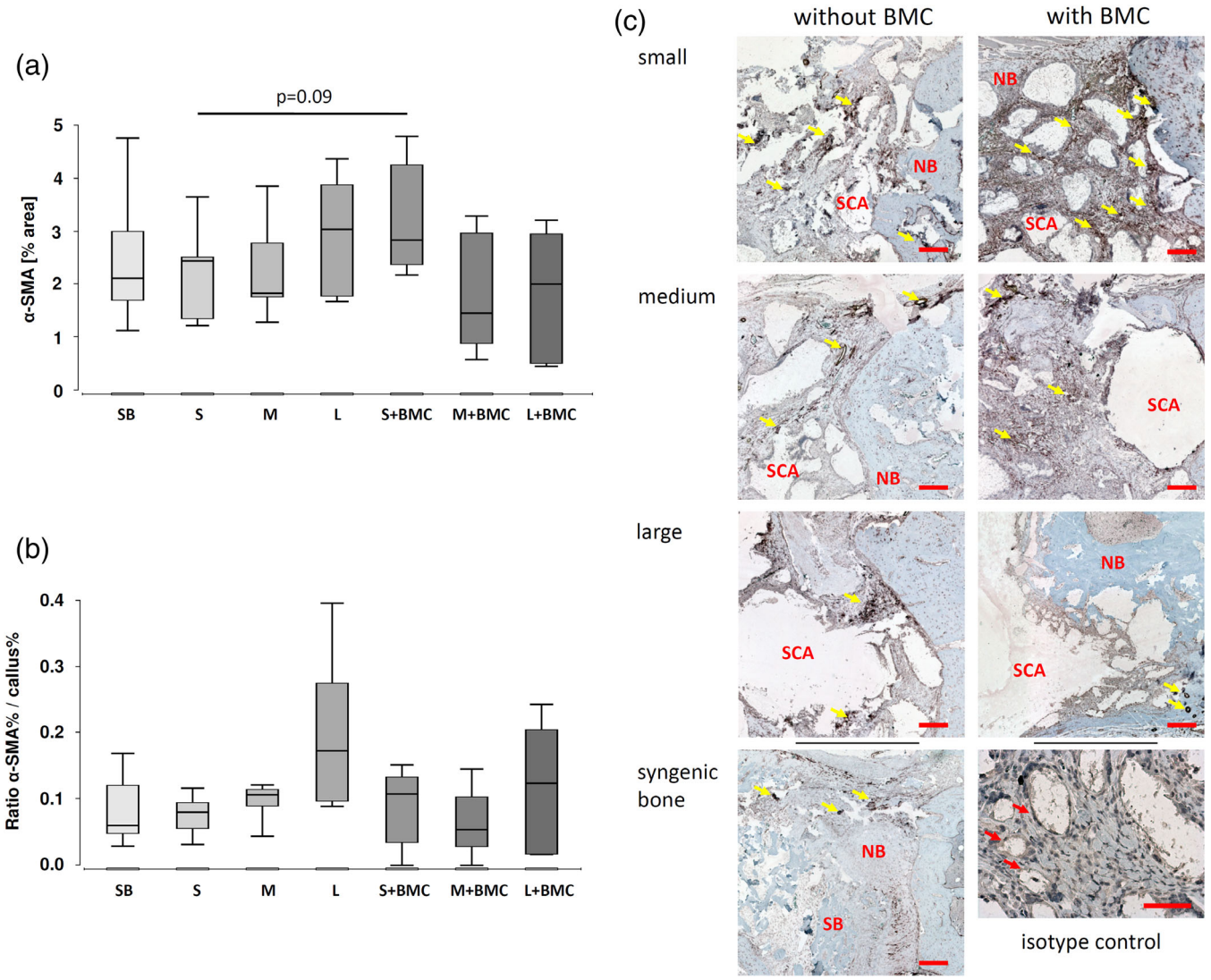

FIGURE 5 α-SMA positive blood vessels within the bone defect in animals transplanted with either small, medium or large sized Herafill granules with or without additional BMC 8 weeks after surgery. Percentage of a-SMA positive area in the defect zone was determined by means of histomorphometry (a). Blood vessels in relation to callus area in the defect zone is presented in (b). Representative images of α-SMA stainings of defects treated without additional BMC (left column) and of additionally BMC treated defects (right column) are provided in (c). Representative isotype control indicating the specificity of the staining is presented in (c, lower row, right image, unstained vessels are marked by red arrows). NB, new bone; Sca, scaffold. Yellow arrows indicate α-SMA positive blood vessels. Red bars represent 500 μm (upper row) with exception of isotype control (50 μm) (isotype control)

compared to syngenic bone respective to small granules. This effect could not be found when BMC were added (Figure 5b).

3.6 | Distribution of macrophage subtypes

Groups with small-sized granules showed the highest count of CD68+ macrophages. Differences between groups with different sized granules were leveled when BMC were added, possibly caused by direct or indirect contribution of the macrophage fraction of the added BMC.

Macrophages are often localized closely to the bone graft substitute which could explain the relatively increased number of macrophages in defects filled with small granules. They were also found in the induced membrane predominantly close to granules and new built bone tissue. The differentiation between M1- (inflammatory subtype, CD80 positive) and M2-macrophages (anti-inflammatory subtype, CD163 positive) was

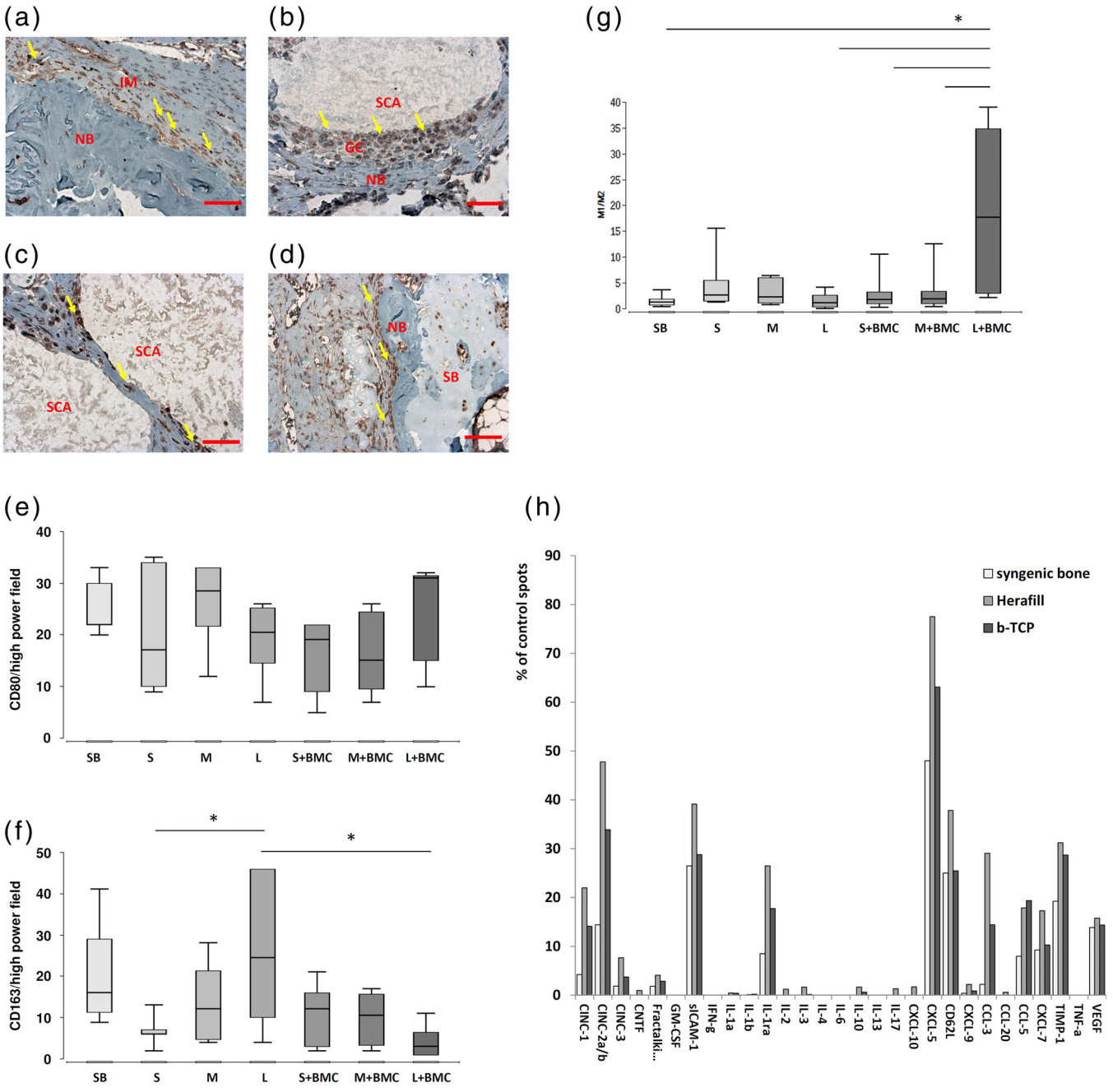

FIGURE 6 Macrophages, location, and distribution within the bone defect. Accumulation of CD68 immunostained macrophages (marked by yellow arrow) in the vicinity of the induced membrane (a), as multinucleated giant cells at the border toward the scaffold granule (b, c) and syngenic bone particles (d). Mean number of M1 macrophages (CD80, e) and of M2 macrophages (CD163, f) per high power field (×400) as well as ratio of M1 to M2 macrophages (g). Representative images were shown in Figures S1 and S2. Whole blood stimulation assay, mediator release to the supernatant after 24 hr incubation of rat whole blood either with small Herafill granules, beta-TCP (ChronOs®) or with syngenic bone is shown in (h). *$p < .05$. GC, giant cell; IM, induced membrane; NB, new bone; SB, syngenic bone; Sca, scaffold. Red bar: a–c: 50 μm, d: 100 μm

done immunohistochemically. A significantly increased number of CD163 positive likely macrophages could be detected in defects filled with large granules without BMC compared to defects filled with small granules. Addition of BMC led to a significant decrease of CD163 positive population when large granules were used (Figure 6f).

Population of CD80 positive inflammatory macrophages did not differ significantly amongst the treatment groups (Figure 6e). The ratio of M1- to M2-macrophages was at a comparable level in all treatment groups with the exception of animals that received large granules loaded with BMC. In this group, a significantly increased ratio of M1- to M2-macrophages was found compared to groups with syngenic bone and large granules without BMC (Figure 6g).

Both M1- and M2-macrophages showed comparable distribution as described for CD68 positive cells. As endothelial cells are able to express both markers, positive cells in local relation to vessels were not taken into account due to coexpression of macrophage marker on endothelial cells.

3.7 | Increased expression of chemotactic and proangiogenic factors in whole blood after incubation with Herafill® granules

Analyzing the stimulatory potential of Herafill® granules an increased release of chemotactic active factors (CINC, CCL3, CXCL5 (LIX), CXCL7), proangiogenic factors (sICAM, VEGF) and a factor involved in tissue remodeling (TIMP-1, Figure 6h) could be observed after incubation of whole blood with small Herafill® (0.5–1.0 mm) compared to syngenic bone. The stimulatory pattern of Herafill granules differed from that of equally sized beta-TCP granules. The latter also stimulates chemotactic factors but generally to a lesser extent compared to Herafill® granules (Figure 6h).

4 | DISCUSSION

We aimed to investigate whether there was an optimum size range for Herafill® granules to support bone healing in a critical size defect in combination with Masquelet's technique and BMC.

We therefore used a critical size defect model in the rodent. Even though the Masquelet technique has been performed in larger models, for example in sheep, most of the published research was done using rats. Christou et al. analyzed ovine induced membrane characteristics and found the expression of BMP2, TGF-b, VEGF, IL-6 to be similar compared to rats' induced membrane (Christou, Oliver, Yu, & Walsh, 2014; Henrich et al., 2016; Nau, Seebach, et al., 2016). Furthermore, also histological aspects of the induced membrane are comparable between rodents and sheep: Christou et al. demonstrate high cell density toward the cement interface, less cells and fibrous tissue oftentimes parallel aligned to the cement interface more distant from the cement spacer. Other and we observed the same structural aspects in the induced membrane of rats.

Herafill® is predominantly used as a carrier for antibiotics in clinical application. However, a clinical study reports new bone formation when granules were implanted in either femoral, tibial, metatarsal or humeral defects (Seyler et al., 2010).

The size of small granules was approximately corresponding to particle size of beta-TCP (Herafill® small: 0.5–1.0 mm, ChronOs®: 0.7–1.4 mm), while the size of medium granules approximately corresponds to the particle size of the autologous bone (1.0–3.0 mm).

Our results showed significant impact of granule size in terms of bone formation and bone mineral density.

Histological analysis showed significantly increased bone formation when small Herafill® granules were used. Qualitatively these results were reproducible in μCT-analysis but not quantitatively. However, this did not necessarily mean complete osseous consolidation of the defect.

Mineralization of the defect zone was also significantly increased when small granules were used. However, compared to healthy bone, BMD was still distinctly lower. Both effects, bone formation and bone mineral density could not be increased by addition of BMC. Possibly, an increased mineralization could have been found after a prolonged healing period.

These results are in line with those of other authors, who found particle size, surface connectivity and packing density between granules of a composite material respectively an allograft-polymer-composite to have influential impact on remodeling and bone formation (Coathup et al., 2013; Prieto et al., 2015).

The newly formed bone was not stable enough for bearing significant biomechanical load after a healing period of 8 weeks. In earlier work, our group was able to yield comparatively good biomechanical properties in a critical size defect-model of a rat's femur when treated with the Masquelet technique and cell-free beta-TCP as a bone void filler (Nau et al., 2018).

An explanation for the low biomechanical properties might be found in the pattern of bone formation. Callus was built predominantly around the single granules within the defect in the form of insular areas that were not confluent after 8 weeks of observation. Material properties might be another reason for the lower stability, Herafill® granules have a lower hardness when compared to beta-TCP.

However, biomechanical stability is only one of many aspects to assess bone healing. Histological and radiological results showed relevant healing progress, even though defects were mineralized to a limited extent compared to healthy bone.

A distinctly increased level of chemokine cytokine ligand 3 (CCL3) was found when small Herafill® granules were incubated with whole blood of the rat (Figure 6h), which might be considered as one possible explanation for the impaired mineralization of the defect. The same experiment has been performed with similarly sized beta-TCP particles. CCL-3 was elevated compared to when syngenic bone was used. However, using Herafill® granules a value twice as high was found. This finding indicates that chemical composition probably influences the mediator release and both, the filler and the calcium sulfate might exert effects.

The role of CCL3 in myeloma-induced bone disease was investigated by Vallet et al. They found osteocalcin expression downregulated and osteoblast mineralization inhibited by CCL3 (Vallet et al., 2011). This observation is confirmed by other authors, who

report CCL3 to impair mineralization in fracture healing and high serum levels of CCL3 to be associated with delayed fracture healing (Edderkaoui, 2017; Fu et al., 2014).

On the other hand, calcium sulfate is also effective in activation of cellular functions by differentially activated Pi3/MAPK pathways (Aquino-Martínez, Angelo, & Pujol, 2017). Specific concentrations are reported to induce bone regeneration in calvarial defects by acting on the host's undifferentiated MSCs and promoting their migration. Following progenitor cell recruitment osteoblast gene expression is increased gradually (Aquino-Martínez et al., 2017).

Analyzing the vascularization within the defect, no significant difference was found between different treatment groups (small, medium, large granules), while addition of BMC led to a slightly higher vascularization when small granules were used. Possibly, differences in vascularization are equalized after 8 weeks. Previous studies of our group showed an increased vascularization activity caused by BMC in early stages of the healing process (Janko et al., 2017). Meanwhile, after 8 weeks, vessel density in the defect zone is significantly decreased (Janko et al., 2019).

The decreased effect of BMC on bone healing and vascularization might be based on the hydrophobic properties of Herafill® and the, therefore, low adhesion of BMC compared to other bone graft substitutes. In order to compensate the decreased seeding efficiency, suspension with nonadherent BMC was additionally dripped into the defect additionally. Even though the induced membrane kept cells at the defect site, they might not have been consistently distributed. However, a consistent distribution within the defect zone and adhesion to the bone graft material might be a basis for consistent effect of BMC.

A further aspect might be that the chemical composition of Herafill® leads to a maximum stimulation of local regenerative capacity in the defect zone which could not be significantly enhanced by addition of BMC. This assumption is supported by comparative observations, for example, that cell-free bone graft substitute based on beta-TCP shows significant bone forming effect only after being enriched with regenerative cells (Seebach et al., 2015).

Herafill® granules consist of calcium sulfate, calcium carbonate and glycerine tripalmitate as bonding additive (Heraeus Medical GmbH, 2017). Palmitate is a saturated nonesterified fatty acid (NEFA) which is known to induce a proinflammatory and immunogenic response in human monocytes and cause synthesis and secretion of IL-6 and TNF-α (Bunn et al., 2010; Riera-Borrull et al., 2017). Furthermore, palmitate increases the secretion of proinflammatory adipokines monocyte chemoattractant protein-1 (MCP-1) and vascular endothelial growth factor (VEGF) (Kitahara et al., 2017). An increased inflammatory potential of Herafill® granules (small) in comparison to syngenic bone could be confirmed in this study. Incubating whole blood of the rat with Herafill® for 24 hr, a distinctly increased release of proangiogenic respective of chemotactic active mediators could be stated in comparison to preparations containing syngenic bone (Figure 6h).

Furthermore, it could be evidenced that increased palmitate-concentration has impact on the polarization of macrophages and their reactivity on inflammatory stimuli via activation of JNK-kinases (Riera-Borrull et al., 2017). Also, evidence is found that high doses of palmitate significantly influence the differentiation of bone marrow-derived macrophages and promote the anti-inflammatory M2-subtype. In already differentiated macrophages, palmitate shows proinflammatory responses (Xiu, Diao, Qi, Catapano, & Jeschke, 2016).

Those effects on monocytes/macrophages are of special interest with regard to the relevance of those cells for regenerative processes. Using subtractive experiments, our group was able to prove, that especially the monocytes within the BMC-preparation are relevant for the formation of new bone tissue (Henrich et al., 2018).

Therefore, based on the findings in earlier work comparing the impact of different sorts of cement Palacos R + G was used to induce the membrane (Nau, Seebach, et al., 2016). Compared to other cements (six were tested), it increases the proportion of vital, cell rich tissue and avital fibrous tissue. The “vital” part of the induced membrane includes macrophages as revealed by immunohistological analysis (Nau, Seebach, et al., 2016).

Macrophages are heterogeneous cells with many subpopulations and partially flowing transitions (Wu, Raggatt, Alexander, & Pettit, 2013). After a fracture, a hematoma develops and is infiltrated by granulocytes, lymphocytes, and monocytes. Different cytokines and chemokines are released by immigrated cells and lead to further recruitment of monocytes/macrophages from circulating monocytes and mesenchymal stem cells from adjacent bone marrow and periosteum (Henrich et al., 2018). Depending on the local environmental conditions in the affected tissue, they are polarized to either M1 or M2-subtype (Ogle, Segar, Sridhar, & Botchwey, 2016).

In this study, the relative number of macrophages (CD68 positive) was significantly increased when small granules were used. Also, macrophages did not show a consistent distribution over the defect area but were predominantly found in the area between granules and bone at the defect site, as well as on the cement-facing side of the induced membrane. Analysis of the subtypes showed a M1/M2-ratio between 1.5 and 4.1 in the treatment groups with the exception of animals that received large granules and BMC. In this group, a significantly increased M1/M2-ratio of 16.2 compared to the groups “syngenic spongiosa” and “Herafill® large without BMC” was found (Figure 6g). Generalizing, a rather proinflammatory polarization of monocytes can be stated for all treatment groups.

It has been described that the early, complete switch toward the anti-inflammatory macrophage subtype M2 within the first week after fracture is necessary for the proper proceeding of the bone healing sequence (Schlundt et al., 2018). In the present study, immunohistological analysis of macrophage subtypes was performed after 8 weeks healing time and thus reliable conclusions about the situation in the early bone defect cannot be drawn. Although, a persisting rather proinflammatory situation in the defect driven by M1 macrophages might contribute to the observed incomplete bone healing. However, further investigations are warranted to elucidate the time course of the M1/M2 development in the defect in presence of granular Herafill®.

5 | CONCLUSION

In conclusion, it can be stated that the granule size of the bone graft substitute Herafill® has significant impact on bone healing of a critical size defect in combination with Masquelet's technique. Granules of the size range of 0.5–1.0 mm showed significantly improved bone healing compared to larger granule sizes, which however did not lead to an increased biomechanical stability in the defect zone. An impact on the vascularization in the defect zone depending on the granule size could not be pointed out after a healing period of 8 weeks. Addition of BMC resulted in only slightly improved vascularization and bone healing parameters. Herafill® (small granules) lead to an increased accumulation of macrophages in situ which could be assigned to the inflammatory subtype M1 by majority. Herafill® granules induced an increased release of chemotactic respectively proangiogenic active factors in vitro compared to syngenic bone and beta-TCP. These activating properties of Herafill® could have resulted in accumulation and polarization of macrophages at the defect site.

DISCLOSURE OF INTERESTS

This project was funded in part by Heraeus Medical GmbH, Wehrheim, Germany. The study sponsor was not involved in data collection or in data analysis and did not influence data interpretation. The sponsor did not decide where the manuscript is submitted.

REFERENCES

Afroz, S., Arakaki, R., Iwasa, T., Oshima, M., Hosoki, M., Inoue, M., … Matsuka, Y. (2019). CGRP induces differential regulation of cytokines from satellite glial cells in trigeminal ganglia and orofacial nociception. *International Journal of Molecular Sciences*, *20*, 711.

Aquino-Martínez, R., Angelo, A. P., & Pujol, F. V. (2017). Calcium-containing scaffolds induce bone regeneration by regulating mesenchymal stem cell differentiation and migration. *Stem Cell Research & Therapy*, *8*, 265.

Bosemark, P., Perdikouri, C., Pelkonen, M., Isaksson, H., & Tägil, M. (2015). The masquelet induced membrane technique with BMP and a synthetic scaffold can heal a rat femoral critical size defect. *Journal of Orthopaedic Research*, *33*, 488–495.

Bunn, R. C., Cockrell, G. E., Ou, Y., Thrailkill, K. M., Lumpkin, C. K., & Fowlkes, J. L. (2010). Palmitate and insulin synergistically induce IL-6 expression in human monocytes. *Cardiovascular Diabetology*, *9*, 73.

Christou, C., Oliver, R. A., Yu, Y., & Walsh, W. R. (2014). The Masquelet technique for membrane induction and the healing of ovine critical sized segmental defects. *PLoS ONE*, *9*, e114122.

Cizkova, D., Cubinkova, V., Smolek, T., Murgoci, A.-N., Danko, J., Vdoviakova, K., … Salzet, M. (2018). Localized intrathecal delivery of mesenchymal stromal cells conditioned medium improves functional recovery in a rat model of spinal cord injury. *International Journal of Molecular Sciences*, *19*, 870.

Coathup, M. J., Cai, Q., Campion, C., Buckland, T., & Blunn, G. W. (2013). The effect of particle size on the osteointegration of injectable silicate-substituted calcium phosphate bone substitute materials. *Journal of Biomedical Materials Research Part B: Applied Biomaterials*, *101*, 902–910.

Coraça-Huber, D. C., Wurm, A., Fille, M., Hausdorfer, J., Nogler, M., Vogt, S., & Kühn, K.-D. (2015). Antibiotic-loaded calcium carbonate/calcium sulfate granules as co-adjuvant for bone grafting. *Journal of Materials Science. Materials in Medicine*, *26*, 5344.

Donegan, D. J., Scolaro, J., Matuszewski, P. E., & Mehta, S. (2011). Staged bone grafting following placement of an antibiotic spacer block for the management of segmental long bone defects. *Orthopedics*, *34*, e730–e735.

Edderkaoui, B. (2017). Potential role of chemokines in fracture repair. *Frontiers in Endocrinology (Lausanne)*, *8*, 39.

Elgström, E., Ohlsson, T. G., & Eriksson, S. E. (2017). Cytokine evaluation in untreated and radioimmunotherapy-treated tumors in an immunocompetent rat model. *Tumour Biology*, *39*, 1010428317697550.

Franceschini, M., Di Matteo, A., Bösebeck, H., Büchner, H., & Vogt, S. (2012). Treatment of a chronic recurrent fistulized tibial osteomyelitis: Administration of a novel antibiotic-loaded bone substitute combined with a pedicular muscle flap sealing. *European Journal of Orthopaedic Surgery and Traumatology*, *22*(Suppl. 1), 245–249.

Fu, R., Liu, H., Zhao, S., Wang, Y., Li, L., Gao, S., … Shao, Z. (2014). Osteoblast inhibition by chemokine cytokine ligand3 in myeloma-induced bone disease. *Cancer Cell International*, *14*, 132.

Garvey, W., Fathi, A., Bigelow, F., Carpenter, B., & Jimenez, C. (1986). Improved Movat pentachrome stain. *Stain Technology*, *61*, 60–62.

Ghanaati, S., Barbeck, M., Orth, C., Willershausen, I., Thimm, B. W., Hoffmann, C., … Kirkpatrick, C. J. (2010). Influence of β-tricalcium phosphate granule size and morphology on tissue reaction in vivo. *Acta Biomaterialia*, *6*, 4476–4487.

Giannoudis, P. V., Faour, O., Goff, T., Kanakaris, N., & Dimitriou, R. (2011). Masquelet technique for the treatment of bone defects: Tips-tricks and future directions. *Injury*, *42*, 591–598.

Gramlich, Y., Walter, G., Gils, J., & Hoffmann, R. (2017). Early results of adjuvant topical treatment of recurrent osteomyelitis with absorbable antibiotic carriers. *Zeitschrift fur Orthopadie und Unfallchirurgie*, *155*, 35–44.

Gupta, G., Ahmad, S., Zahid, M., Khan, A. H., Sherwani, M. K. A., & Khan, A. Q. (2016). Management of traumatic tibial diaphyseal bone defect by "induced-membrane technique". *Indian Journal of Orthopaedics*, *50*, 290–296.

Henrich, D., Seebach, C., Kaehling, C., Scherzed, A., Wilhelm, K., Tewksbury, R., … Marzi, I. (2009). Simultaneous cultivation of human endothelial-like differentiated precursor cells and human marrow stromal cells on beta-tricalcium phosphate. *Tissue Engineering Part C Methods*, *15*, 551–560.

Henrich, D., Seebach, C., Nau, C., Basan, S., Relja, B., Wilhelm, K., … Marzi, I. (2016). Establishment and characterization of the Masquelet induced membrane technique in a rat femur critical-sized defect model. *Journal of Tissue Engineering and Regenerative Medicine*, *10*, E382–E396.

Henrich, D., Seebach, C., Verboket, R., Schaible, A., Marzi, I., & Bonig, H. (2018). The osteo-inductive activity of bone-marrow-derived mononuclear cells resides within the CD14+ population and is independent of the CD34+ population. *European Cells & Materials*, *35*, 165–177.

Heraeus Medical GmbH. HERAFILL. Heraeus Medical GmbH editor. https://www.heraeus.commediamediahmedochmeproductshmeherafillheraeusHERAFILLFolderEN.pdf. Werheim, Germany; [cited 2017 Nov 28]. Retrieved from https://www.heraeus.commediamediahmedochmeproductshmeherafillheraeusHERAFILLFolderEN.pdf.

Janko, M., Dietz, K., Rachor, J., Sahm, J., Schröder, K., Schaible, A., … Henrich, D. (2019). Improvement of bone healing by neutralization of microRNA-335-5p, but not by neutralization of microRNA-92A in bone marrow mononuclear cells transplanted into a large femur defect of the rat. *Tissue Engineering. Part A*, *25*, 55–68.

Janko, M., Sahm, J., Schaible, A., Brune, J. C., Bellen, M., Schröder, K., … Henrich, D. (2017). Comparison of three different types of scaffolds preseeded with human bone marrow mononuclear cells on the bone healing in a femoral critical size defect model of the athymic rat. *Journal of Tissue Engineering and Regenerative Medicine*, *106*, 3009.

Jensen, S. S., Aaboe, M., Janner, S. F. M., Saulacic, N., Bornstein, M. M., Bosshardt, D. D., & Buser, D. (2015). Influence of particle size of deproteinized bovine bone mineral on new bone formation and implant stability after simultaneous sinus floor elevation: A histomorphometric study in minipigs. *Clinical Implant Dentistry and Related Research*, *17*, 274–285.

Kitahara, A., Takahashi, K., Morita, N., Murashima, T., Onuma, H., Sumitani, Y., … Ishida, H. (2017). The novel mechanisms concerning the inhibitions of palmitate-induced proinflammatory factor releases and endogenous cellular stress with Astaxanthin on MIN6 β-cells. *Marine Drugs*, *15*, 185.

Klüppel, L. E., Antonini, F., Olate, S., Nascimento, F. F., Albergaria-Barbosa, J. R., & Mazzonetto, R. (2013). Bone repair is influenced by different particle sizes of anorganic bovine bone matrix: A histologic and radiographic study in vivo. *The Journal of Craniofacial Surgery*, *24*, 1074–1077.

Kon, K., Shiota, M., Ozeki, M., & Kasugai, S. (2014). The effect of graft bone particle size on bone augmentation in a rabbit cranial vertical augmentation model: A microcomputed tomography study. *The International Journal of Oral & Maxillofacial Implants*, *29*, 402–406.

Malinin, T. I., Carpenter, E. M., & Temple, H. T. (2007). Particulate bone allograft incorporation in regeneration of osseous defects; importance of particle sizes. *The Open Orthopaedics Journal*, *1*, 19–24.

Marczak, D., Synder, M., Sibiński, M., Okoń, T., & Kowalczewski, J. (2016). The use of calcium carbonate beads containing gentamicin in the second stage septic revision of total knee arthroplasty reduces reinfection rate. *The Knee*, *23*, 322–326.

Masquelet, A. C., & Begue, T. (2010). The concept of induced membrane for reconstruction of long bone defects. *Orthopedic Clinics of North America*, *41*, 27–37.

Masquelet, A. C., Fitoussi, F., Begue, T., & Muller, G. P. (2000). Reconstruction of the long bones by the induced membrane and spongy autograft. *Annales de Chirurgie Plastique et Esthétique*, *45*, 346–353.

Maté Sánchez de Val, J. E., Calvo-Guirado, J. L., Gómez-Moreno, G., Pérez-Albacete Martínez, C., Mazón, P., & De Aza, P. N. (2016). Influence of hydroxyapatite granule size, porosity, and crystallinity on tissue reaction in vivo. Part A: Synthesis, characterization of the materials, and SEM analysis. *Clinical Oral Implants Research*, *27*, 1331–1338.

Moghaddam, A., Zietzschmann, S., Bruckner, T., & Schmidmaier, G. (2015). Treatment of atrophic tibia non-unions according to "diamond concept": Results of one- and two-step treatment. *Injury*, *46*(Suppl. 4), S39–S50.

Nau, C., Henrich, D., Seebach, C., Schröder, K., Fitzsimmons, S.-J., Hankel, S., … Frank, J. (2016). Treatment of large bone defects with a vascularized periosteal flap in combination with biodegradable scaffold seeded with bone marrow-derived mononuclear cells: An experimental study in rats. *Tissue Engineering. Part A*, *22*, 133–141.

Nau, C., Seebach, C., Trumm, A., Schaible, A., Kontradowitz, K., Meier, S., … Henrich, D. (2016). Alteration of Masquelet's induced membrane characteristics by different kinds of antibiotic enriched bone cement in a critical size defect model in the rat's femur. *Injury*, *47*, 325–334.

Nau, C., Simon, S., Schaible, A., Seebach, C., Schröder, K., Marzi, I., & Henrich, D. (2018). Influence of the induced membrane filled with syngeneic bone and regenerative cells on bone healing in a critical size defect model of the rat's femur. *Injury*, *49*, 1721–1731.

Ogle, M. E., Segar, C. E., Sridhar, S., & Botchwey, E. A. (2016). Monocytes and macrophages in tissue repair: Implications for immunoregenerative biomaterial design. *Experimental Biology and Medicine (Maywood, NJ)*, *241*, 1084–1097.

Pförringer, D., Obermeier, A., Kiokekli, M., Büchner, H., Vogt, S., Stemberger, A., … Lucke, M. (2016). Antimicrobial formulations of absorbable bone substitute materials as drug carriers based on calcium sulfate. *Antimicrobial Agents and Chemotherapy*, *60*, 3897–3905.

Prieto, E. M., Talley, A. D., Gould, N. R., Zienkiewicz, K. J., Drapeau, S. J., Kalpakci, K. N., & Guelcher, S. A. (2015). Effects of particle size and porosity on in vivo remodeling of settable allograft bone/polymer composites. *Journal of Biomedical Materials Research Part B: Applied Biomaterials*, *103*, 1641–1651.

Putzer, D., Coraça-Huber, D., Wurm, A., Schmoelz, W., & Nogler, M. (2014). Optimizing the grain size distribution of allografts in bone impaction grafting. *Journal of Orthopaedic Research*, *32*, 1024–1029.

Riera-Borrull, M., Cuevas, V. D., Alonso, B., Vega, M. A., Joven, J., Izquierdo, E., & Corbí, Á. L. (2017). Palmitate conditions macrophages for enhanced responses toward inflammatory stimuli via JNK activation. *Journal of Immunology*, *199*, 3858–3869.

Schemitsch, E. H. (2017). Size matters: Defining critical in bone defect size. *Journal of Orthopaedic Trauma*, *31*(Suppl. 5), S20–S22.

Schlundt, C., Khassawna El, T., Serra, A., Dienelt, A., Wendler, S., Schell, H., … Schmidt-Bleek, K. (2018). Macrophages in bone fracture healing: Their essential role in endochondral ossification. *Bone*, *106*, 78–89.

Seebach, C., Henrich, D., Kähling, C., Wilhelm, K., Tami, A. E., Alini, M., & Marzi, I. (2010). Endothelial progenitor cells and mesenchymal stem cells seeded onto beta-TCP granules enhance early vascularization and bone healing in a critical-sized bone defect in rats. *Tissue Engineering. Part A*, *16*, 1961–1970.

Seebach, C., Henrich, D., Meier, S., Nau, C., Bönig, H., & Marzi, I. (2016). Safety and feasibility of cell-based therapy of autologous bone marrow-derived mononuclear cells in plate-stabilized proximal humeral fractures in humans. *Journal of Translational Medicine*, *14*, 314.

Seebach, C., Henrich, D., Schaible, A., Relja, B., Jugold, M., Bönig, H., & Marzi, I. (2015). Cell-based therapy by implanted human bone marrow-derived mononuclear cells improved bone healing of large bone defects in rats. *Tissue Engineering. Part A*, *21*, 1565–1578.

Seebach, C., Henrich, D., Wilhelm, K., Barker, J. H., & Marzi, I. (2012). Endothelial progenitor cells improve directly and indirectly early vascularization of mesenchymal stem cell-driven bone regeneration in a critical bone defect in rats. *Cell Transplantation*, *21*, 1667–1677.

Seebach, C., Schultheiss, J., Wilhelm, K., Frank, J., & Henrich, D. (2010). Comparison of six bone-graft substitutes regarding to cell seeding efficiency, metabolism and growth behaviour of human mesenchymal stem cells (MSC) in vitro. *Injury*, *41*, 731–738.

Seyler, T. M., Boesebeck, H., Buechner, H., Vogt, S., Hofmann, R., Walter, G., … Kiokekli M. Preclinical and clinical experience of a novel calcium sulfate/carbonate based bone substitute with antibiotic release. *56th Annual Meeting of the Orthopaedic Research Society*; 2010.

Shapoff, C. A., Bowers, G. M., Levy, B., Mellonig, J. T., & Yukna, R. A. (1980). The effect of particle size on the osteogenic activity of composite grafts of allogeneic freeze-dried bone and autogenous marrow. *Journal of Periodontology*, *51*, 625–630.

Sun, J. S., Lin, F. H., Hung, T. Y., Tsuang, Y. H., Chang, W. H., & Liu, H. C. (1999). The influence of hydroxyapatite particles on osteoclast cell activities. *Journal of Biomedical Materials Research*, *45*, 311–321.

Vallet, S., Pozzi, S., Patel, K., Vaghela, N., Fulciniti, M. T., Veiby, P., … Raje, N. (2011). A novel role for CCL3 (MIP-1α) in myeloma-induced bone disease via osteocalcin downregulation and inhibition of osteoblast function. *Leukemia*, *25*, 1174–1181.

Verboket, R., Leiblein, M., Seebach, C., Nau, C., Janko, M., Bellen, M., … Marzi, I. (2018). Autologous cell-based therapy for treatment of large bone defects: From bench to bedside. *European Journal of Trauma and Emergency Surgery*, *9*, 1–17.

Warzecha, J., Seebach, C., Flinspach, A., Wenger, F., Henrich, D., & Marzi, I. (2013). Effect of sonic hedgehog/β-TCP composites on bone healing within the critical-sized rat femoral defect. *Experimental and Therapeutic Medicine*, *5*, 1035–1039.

Wiese, A., & Pape, H. C. (2010). Bone defects caused by high-energy injuries, bone loss, infected nonunions, and nonunions. *Orthopedic Clinics of North America*, *41*, 1–4.

Wu, A. C., Raggatt, L. J., Alexander, K. A., & Pettit, A. R. (2013). Unraveling macrophage contributions to bone repair. *Bonekey Reports*, *2*, 373.

Xiu, F., Diao, L., Qi, P., Catapano, M., & Jeschke, M. G. (2016). Palmitate differentially regulates the polarization of differentiating and differentiated macrophages. *Immunology*, *147*, 82–96.

SUPPORTING INFORMATION

Additional supporting information may be found online in the Supporting Information section at the end of this article.

How to cite this article: Leiblein M, Koch E, Winkenbach A, et al. Size matters: Effect of granule size of the bone graft substitute (Herafill®) on bone healing using Masquelet's induced membrane in a critical size defect model in the rat's femur. *J Biomed Mater Res*. 2020;108B:1469–1482. https://doi.org/10.1002/jbm.b.34495